Identification of *A*- and *B*-Site Cation Vacancy Defects in Perovskite Oxide Thin Films

D. J. Keeble,[1,*] S. Wicklein,[2] R. Dittmann,[2] L. Ravelli,[2] R. A. Mackie,[1] and W. Egger[3]

[1]*Carnegie Laboratory of Physics, School of Engineering, Physics, and Mathematics, University of Dundee, Dundee DD1 4HN, United Kingdom*

[2]*Institut für Festköperforschung, Forschungszentrum Jülich, 52425 Jülich, Germany*

[3]*Universität Bundeswehr München, D-85577 Neubiberg, Germany*

(Received 31 August 2010; published 23 November 2010)

Cation vacancies on both sublattices (V_{Ti}, V_{Sr}) have been identified in homoepitaxial pulsed laser deposited $SrTiO_3$ films using high intensity variable energy positron annihilation lifetime spectroscopy (PALS) measurements. Film nonstoichiometry was varied by varying laser fluence. PALS showed that on increasing the fluence above the $Ti/Sr \sim 1$ value, the concentration ratio $[V_{Sr}]/[V_{Ti}]$ systematically increased. Reducing the fluence into the Ti-poor region below resulted in additional vacancy cluster defect formation. Vacancy concentrations greater than ~50 ppm were observed in all films.

DOI: 10.1103/PhysRevLett.105.226102 PACS numbers: 68.55.Ln, 61.72.jd, 77.84.−s, 78.70.Bj

The extraordinary breadth of fundamental properties exhibited by complex oxides establishes their position as emergent research device materials [1]. This diversity is largely confined to perovskite oxide, ABO_3, related materials, thus enabling growth of epitaxial multilayers with well-defined interfaces. Films with conductivities from insulating to superconducting can be combined with ferroelectric, piezoelectric, magnetic, or multiferroic, layers. The control of conducting electron systems at interfaces between $SrTiO_3$ and other band insulators provides further novel device design opportunities [2]. Device materials, however, typically require unparalleled levels of purity and perfection. This presents a particular challenge for oxides, imposing severe demands on stoichiometry and impurity content, which in turn require suitable characterization methods with concomitant sensitivity. The dominant native point defects in the close packed ABO_3 structure are expected to be vacancies. Point and extended defects in oxides often influence, and can control, both transport and the characteristic physical property, e.g., ferroelectricity, providing opportunities for nanoscale engineering [3,4]. While the importance of oxygen nonstoichiometry in oxide epilayers has been established [5], the existence and nature of cation nonstoichiometry has received less attention. Recently, however, its central role in the suppression of donor doping activity in $SrTiO_3$ was demonstrated [6,7].

Here we report the detection and identification of both Ti and Sr vacancies in pulsed laser deposited (PLD) homoepitaxial $SrTiO_3$ using depth resolved positron lifetime measurements made with a high intensity, reactor-based, positron beam. Defect identification is confirmed by density functional theory (DFT) calculations of positron lifetimes. These calculations are extended to other complex oxides and illustrate the broad potential of the method.

PLD is widely used for producing high quality complex oxide thin films, in part due to its perceived simplicity. While it is often assumed that transfer from the ceramic target is stoichiometric, it has been demonstrated that the $SrTiO_3$ Ti/Sr ratio can vary with laser fluence [6,8]. Molecular beam epitaxy deposition of $SrTiO_3$ has been performed using solid sources where fluxes, and hence stoichiometry, can be controlled to on the order of 0.1%–1% [9], and with a combination of solid and metal-organic sources where precision may be improved by self-regulation of stoichiometry [7]. Variation in Ti/Sr ratios has been inferred from variation of the *c*-axis lattice expansion with respect to the substrate, measured using high-resolution x-ray diffraction (XRD) [6,8–10]. Stoichiometry has been quantified using Rutherford backscattering spectroscopy; films exhibiting an XRD peak coincident with the substrate and designated stoichiometric deviated by $<1\%$ in composition, films with $\Delta c \leq 5.5$ pm deviated by $<5\%$ [9]. Energy-dispersive x-ray spectroscopy (EDS) of PLD films established a variation in stoichiometry from Ti poor at low laser fluence, through $Ti/Sr \sim 1$, to Sr poor at high fluence; films with expansions of 13 and 0.4 pm gave Sr excesses of 21.8% and 1.0%, respectively, increasing the fluence further gave a film with $\Delta c = 5$ pm and a Ti excess of 4.5% [8].

When the cation nonstoichiometry is large transmission electron microscopy (TEM) identifies Ruddlesden-Popper planar faults for Sr excess [6,9,11], or regions of amorphous TiO_2 for Ti excess [11]. The possible presence of cation vacancies has been inferred from inhomogeneous contrast modulations observed from films with smaller Ti excess [6]. However, TEM is limited to the detection of local vacancy concentrations of the order ~1% [5], and while EDS can provide Sr/Ti ratios with comparable sensitivity, it cannot recognize the coexistence of Ti and Sr vacancies. The presence of cation vacancy defects has also been inferred using electron spectroscopy methods; electron energy loss near-edge structure in combination with theoretical calculations suggest the presence of V_{Sr} defects at $SrTiO_3$ grain boundaries [12], and x-ray

absorption spectroscopy of TiO_2: Nb showed an increase in Ti 3*d* holes attributed to Ti vacancies [13].

Positron lifetime measurements can have sub-ppm sensitivity for vacancy defects [14], and can provide defect identification. Implanted positrons rapidly thermalize, then annihilate from a state i with a lifetime τ_i and probability I_i. This can be a delocalized state in perfect lattice, or a localized state at a vacancy defect since positrons can trap strongly in the potential well resulting from the missing atomic core. The reduced electron density at the vacancy site increases the positron lifetime above the value characteristic of the perfect (bulk) material τ_b (Table I). The positron annihilation lifetime spectroscopy (PALS) spectrum contains multiexponential lifetime components convolved with the spectrometer timing resolution function, and is analyzed using a trapping model where the rate of positron trapping κ_V is proportional to the defect concentration $[V]$, $\kappa_V = \mu_V[V]$; μ_V is the defect specific trapping coefficient [14]. If there is only one type of vacancy, then two lifetime components are predicted; the second, $\tau_2 = \tau_d$, is characteristic of the particular vacancy (e.g., Table I), and the first has a value depressed below the perfect lattice lifetime by an amount that depends on the rate of trapping to the defect, $\tau_1 \leq \tau_B$. At sufficiently high defect concentrations τ_1 becomes negligible and cannot be detected. This indicates the onset of saturation trapping and sets the upper limit for the *absolute* vacancy concentration that can determined by lifetime measurements. However, if the positron diffusion length can be measured, this limit can be circumvented. When two types of vacancy defect are present, e.g., V_1 and V_2, and saturation trapping occurs, the ratio of the intensities of the two defect lifetime components is given by

$$\frac{I_1}{I_2} = \left(\frac{\mu_{V_1}}{\mu_{V_2}}\right)\left(\frac{[V_1]}{[V_2]}\right). \quad (1)$$

The μ_V value depends on the local charge of the vacancy defect; neutral or negative vacancies are efficient positron traps, positively charged vacancies normally show negligible trapping [15]. The temperature dependence of μ_V also depends on vacancy local charge, positron trapping to negative vacancies increases with decreasing temperature, while trapping to positive vacancies would decrease rapidly [15].

TABLE I. Calculated positron lifetimes (ps) for perfect lattice (bulk) and monovacancy defects in selected ABO_3 and related materials.

Material	Bulk	Defect structure	V_A	V_B	V_O
$PbTiO_3$	161	Unrelaxed	292	204	165
		Relaxed	290	185	
$SrTiO_3$	152	Unrelaxed	280	195	161
		Relaxed	281	189	
$SrRuO_3$	150	Unrelaxed	288	200	161
$Sr_3Ru_2O_7$	180	Unrelaxed	301	207	187
$LaMnO_3$	145	Unrelaxed	282	196	158
$TbMnO_3$	152	Unrelaxed	259	199	161
$BiFeO_3$	154	Unrelaxed	290	198	161

$SrTiO_3$ films were deposited by PLD on $SrTiO_3$ (001) substrates using KrF excimer laser, the laser fluence was varied between 1.00–2.50 $J\,cm^{-2}$. Films were grown in 0.25 mbar oxygen with a substrate temperature of 720 °C then cooled in 0.25 mbar oxygen [16]. The rate per laser shot was ~0.03 nm at 2.00 $J\,cm^{-2}$, and the films were ~200 nm thick. Atomic force microscopy showed that the 1.67–2.50 $J\,cm^{-2}$ films exhibited smooth step-terrace structure confirming layer-by-layer growth, lower fluence values resulted in island growth. The *c*-axis lattice parameter expansion was determined by fitting the $SrTiO_3$ (002) XRD Cu-$K_{\alpha 1}$ peaks for the substrate and the film using Voigt functions [8,16]. Variable energy (VE) PALS measurements were performed on films grown with laser fluences in the range 1.50–2.00 $J\,cm^{-2}$ at the neutron induced positron source (NEPOMUC) at the Munich research reactor FRMII [17,18]. The positron beam energy was varied between 1 and 18 keV, and each lifetime spectra contained $>5 \times 10^6$ counts accumulated with a count rate of $\sim 6 \times 10^3$ s^{-1}. The instrument timing resolution function was normally described by three dominant, energy dependent, terms; these showed a mean width, averaged over all energies, of 299(20) ps. Three lifetime component fits were found to give the best χ^2 values; the mean for all the fit values was 1.14(8). The third lifetime component had an average intensity <0.62% in all the films and is not shown. DFT calculations were performed using the MIKA/DOPPLER package [19], using the Arponen and Pajanne electron-positron enhancement factor described within the generalized gradient approximation [16,20]. Conventional PALS measurements were performed on top seed solution grown $SrTiO_3$ and $SrTiO_3$: Nb crystals between 12–300 K, as described elsewhere [21].

DFT calculated positron lifetimes in perovskite oxides are typically in the range 150–160 ps for perfect lattice, 190–200 ps for the six-coordinated *B*-site monovacancy, and 280–290 ps for the more open 12-coordinated *A*-site vacancy [21–23]. The lifetimes for vacancy defects on the three lattice sites are clearly separated and can provide unambiguous defect identification. Here these calculations are extended to selected conducting, magnetic, and multiferroic perovskite oxide related materials, $SrRuO_3$, $Sr_3Ru_2O_7$, $LaMnO_3$, $TbMnO_3$, and $BiFeO_3$, and the same trends are observed (Table I). Local relaxation of the neighbor atoms can alter the vacancy defect lifetime; calculations for the relaxed cation vacancy structures in $SrTiO_3$ and $PbTiO_3$ are also given [23,24]. The V_{Ti} near neighbor relaxations significantly decrease the positron lifetime, while the similar, but smaller, V_{Sr} site relaxations have a negligible effect (Table I). Calculated lifetime values for V_A-V_O complexes are only slightly greater (~ 4 ps) than isolated cation vacancy values [21–23]. In contrast, V_B-V_O complex lifetimes are ~20–30 ps greater [21,22], and should be readily detected.

The measured c-axis lattice expansions with respect to the substrate (390.5 pm) as a function of laser fluence are shown in Fig. 1(a). This is consistent with previous studies [6,8–10], and it can be inferred that the stoichiometry varies from Ti poor, through Ti/Sr ~ 1 at 1.50 J cm^{-2}, to Sr poor with increasing fluence. Figure 1(a) also shows the mean positron lifetimes for the films, averaged over the 3–5 keV positron implantation energy range [16]. The minimum occurred for the 1.50 J cm^{-2} film, then increased systematically in the Sr-poor region (1.50–2.00 J cm^{-2}). The form of the lifetime component depth profiles were similar in this region [16]; the 1.67 J cm^{-2} results are shown in Figs. 2(a) and 2(b). Below 3 keV (~ 40 nm), the second lifetime value increased indicating a contribution from larger vacancy complex defects in the near surface region. At 5 keV the implantation profile is confined to the film [Fig. 2(c)]; as implantation energy increases, the contribution from the substrate systematically increases causing a reduction in the resolved lifetime values [Fig. 2(a)].

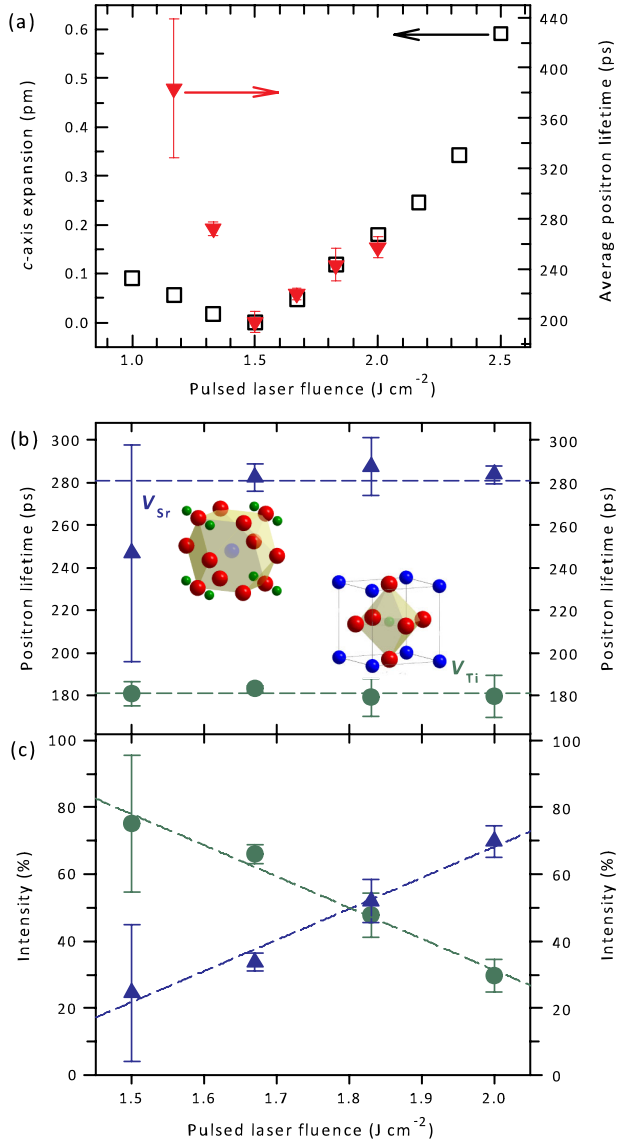

FIG. 1 (color online). (a) The $SrTiO_3$ film c-axis parameter expansion derived from XRD 2θ-ω scans of the (002) peak (square symbols) and the mean positron lifetime (triangle) (1–5 keV implantation range average), as a function of PLD laser fluence. (b) The component positron lifetimes and (c) intensities for the 1.50–2.00 J cm^{-2} films (3–5 keV average). The V_{Ti} and V_{Sr} lifetimes, 181 and 281 ps, respectively, are shown in (b).

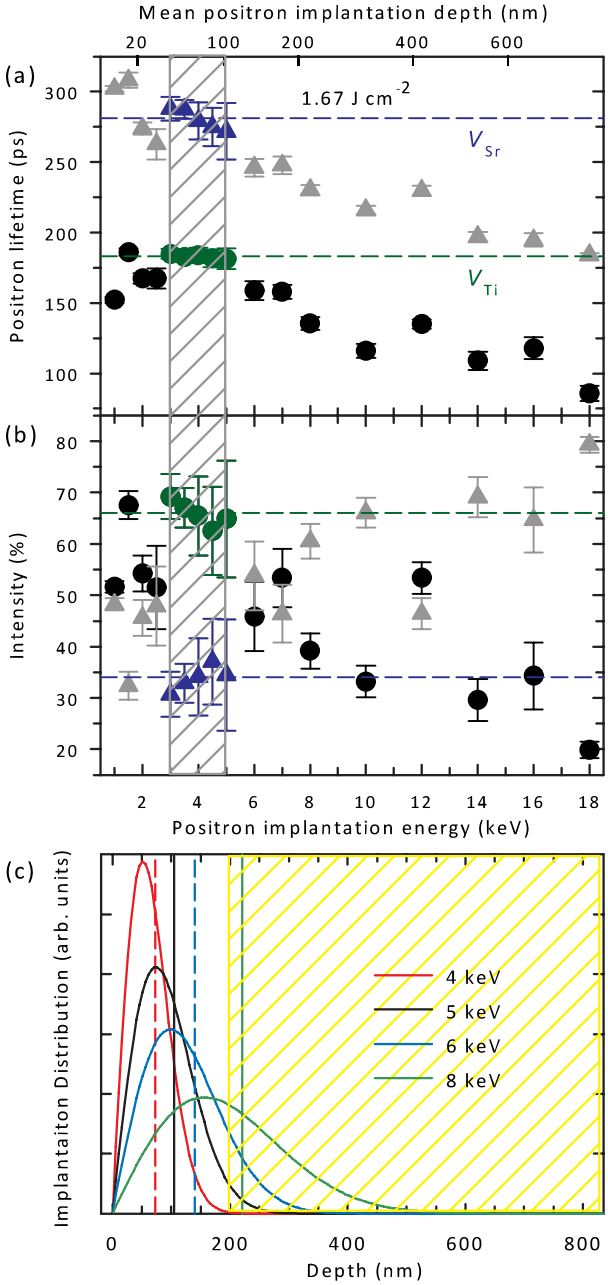

FIG. 2 (color online). Depth profiled positron lifetime components for the 1.67 J cm^{-2} $SrTiO_3$ film. (a) Lifetimes (dashed lines denote 181 and 281 ps), (b) intensities with positron implantation energy. The dashed lines denote the 3–5 keV (gray shading) average values. (c) The Makhovian positron implantation profiles [substrate denoted by gray (yellow) shading].

The positron lifetime and intensity values for the 1.50–2.00 J cm^{-2} films, obtained by averaging 3–5 keV, are shown in Figs. 1(b) and 1(c). Two vacancy defect lifetimes, ~280 and ~181 ps, were clearly resolved and in good agreement with crystal $SrTiO_3$ measurements and the DFT lifetime values for V_{Sr} and V_{Ti}, respectively (Table I) [21].

Earlier PALS on crystal $SrTiO_3$ observed positron trapping to a vacancy defect with a lifetime of 181(3) ps at low temperatures; the strong increase in trapping with decreasing temperature showed the vacancy had a negative local charge supporting the identification as the Ti vacancy [21]. These measurements were extended in this work to top seed solution grown crystals, and temperature independent saturation trapping at a single 180(2) ps vacancy defect, V_{Ti}, was observed. Low temperature measurements were also performed on Nb-doped crystals, and an increase in trapping to a 278(7) ps vacancy defect, V_{Sr}, was observed. Positron lifetime measurements on $Pb(Zr_{0.4}Ti_{0.6})O_3$ (PZT) ceramics and $PbTiO_3$ crystals and doped ceramics also consistently observed vacancy defects at ~180 and ~290 ps due to V_B and V_A defects, respectively [22,23]. At low temperatures there was a marked increase in the V_B intensity, due to more rapid increase in $\mu_{V_B}(T)$ with decreasing temperature resulting from the larger negative charge (V_B^{4-}, V_A^{2-}) [15].

The intensity of the V_{Sr} lifetime component shown in Fig. 1(c) was observed to systematically increase with laser fluence, consistent with the expected increase in the Ti/Sr ratio from ~1 at 1.50 J cm^{-2} [Fig. 1(a)]. The vacancy defect concentrations were above the saturation trapping limit in all samples, and the intensity variation can be described by Eq. (1). The dominant trapping to V_{Ti} for Ti/Sr ~ 1($[V_{Ti}] \approx [V_{Sr}]$) is consistent with $\mu_{V_{Ti}} > \mu_{V_A}$ [21,22]. Further, from the observation of $I_{V_{Ti}}/I_{V_{Sr}} \approx 3.6$ at 1.5 J cm^{-2} [Fig. 1(c)], where it is inferred that $[V_{Ti}] \approx [V_{Sr}]$ [Fig. 1(a)], it follows from Eq. (1) that this is also the ratio of the defect specific trapping coefficients ($\mu_{V_{Ti}}/\mu_{V_{Sr}} \approx 3.6$). Considering the difference in local charge (V_{Ti}^{4-}, V_{Sr}^{2-}), this is a plausible value [14,15].

Reducing the fluence into the Ti-poor, Ti/Sr < 1, region resulted in a rapid increase in the mean lifetime [Fig. 1(a)]. The second lifetime component in the film increased to ~377(10) ps in the 1.33 J cm^{-2} film and to ~410(21) ps in the 1.17 J cm^{-2} film [16], and is due to the formation of vacancy cluster defects [25]. Similar defects were detected in an initial VE-PALS study of a $SrTiO_3$ PLD film [25].

In conclusion, both Sr and Ti vacancy defects have been observed in a series of PLD $SrTiO_3$ films grown with varying laser fluence, and hence stoichiometry, using depth profiling positron annihilation lifetime spectroscopy. Positron trapping at V_{Sr} defects with a lifetime of ~280 ps, and V_{Ti} defects at 181 ps, were clearly resolved and agreed with the DFT calculated values and bulk $SrTiO_3$ single crystal results. The intensity of trapping to V_{Sr} defects increased with increasing PLD laser fluence and film c-axis lattice parameter expansion. These thin film measurements were made possible due to the combination of an intense reactor-based variable energy positron beam with a pulsed positron lifetime spectrometer [17,18]. VE PALS has a sensitivity limit on the order of 0.1 ppm for negative cation vacancy defects; previously the presence of vacancy defects in thin film oxides has been inferred from TEM and electron spectroscopy where defect concentrations of 1%–10% are required [5,6,13]. All the $SrTiO_3$ films studied had cation vacancy defect concentrations greater than ~50 ppm. The DFT calculations were extended to the range of relevant perovskite oxides and showed that the vacancy defects had well separated positron lifetime values similar to $SrTiO_3$. This work provides evidence that VE PALS is capable of sensitive detection and characterization of vacancy defects in a wide range of oxide thin films and multilayers.

D. J. K. acknowledges European Commission Programme RII3-CT-2003-505925. We thank C. Hugenschmidt for providing the NEUPOMUC beam line. D. J. K. thanks I. Makkonen, Helsinki University of Technology, for MIKA/DOPPLER support.

*d.j.keeble@dundee.ac.uk

[1] H. Takagi and H. Y. Hwang, Science **327**, 1601 (2010).
[2] J. Mannhart and D. G. Schlom, Science **327**, 1607 (2010).
[3] K. Szot *et al.*, Nature Mater. **5**, 312 (2006).
[4] S. V. Kalinin *et al.*, Adv. Mater. **22**, 314 (2010).
[5] D. A. Muller *et al.*, Nature (London) **430**, 657 (2004).
[6] T. Ohnishi *et al.*, J. Appl. Phys. **103**, 103703 (2008).
[7] J. Son *et al.*, Nature Mater. **9**, 482 (2010).
[8] T. Ohnishi *et al.*, Appl. Phys. Lett. **87**, 241919 (2005).
[9] C. M. Brooks *et al.*, Appl. Phys. Lett. **94**, 162905 (2009).
[10] B. Jalan, P. Moetakef, and S. Stemmer, Appl. Phys. Lett. **95**, 032906 (2009).
[11] T. Suzuki, Y. Nishi, and M. Fujimoto, Philos. Mag. A **80**, 621 (2000).
[12] T. Mizoguchi *et al.*, Appl. Phys. Lett. **87**, 241920 (2005).
[13] S. X. Zhang *et al.*, Adv. Mater. **21**, 2282 (2009).
[14] R. Krause-Rehberg, and H. S. Leipner, *Positron Annihilation in Semiconductors* (Springer-Verlag, Berlin, 1999).
[15] M. J. Puska, C. Corbel, and R. M. Nieminen, Phys. Rev. B **41**, 9980 (1990).
[16] See supplementary material at http://link.aps.org/supplemental/10.1103/PhysRevLett.105.226102 for details on DFT calculations and VE-PALS results.
[17] P. Sperr *et al.*, Appl. Surf. Sci. **255**, 35 (2008).
[18] C. Hugenschmidt *et al.*, Nucl. Instrum. Methods Phys. Res., Sect. A **593**, 616 (2008).
[19] T. Torsti *et al.*, Phys. Status Solidi B **243**, 1016 (2006).
[20] B. Barbiellini *et al.*, Phys. Rev. B **53**, 16 201 (1996).
[21] R. A. Mackie *et al.*, Phys. Rev. B **79**, 014102 (2009).
[22] D. J. Keeble *et al.*, Phys. Rev. B **76**, 144109 (2007).
[23] R. A. Mackie, A. Pelaiz-Barranco, and D. J. Keeble, Phys. Rev. B **82**, 024113 (2010).
[24] T. Tanaka *et al.*, Phys. Rev. B **68**, 205213 (2003).
[25] D. J. Keeble *et al.*, Phys. Rev. B **81**, 064102 (2010).